WEP Warwick Evans Publishing

International Journal of Natural Resources and Environmental Studies

ISSN: 3006-2012 (Print), ISSN: 3006-0834 (Online) | Volume 2, Number 1, Year 2024
DOI: https://doi.org/10.62051/ijnres.v2n1.25
Journal homepage: https://wepub.org/index.php/IJNRES/index

Research on Extracting Multiple Feature Impervious Surface Based on Fusion of Optics and Radar

Libo Deng, Jiabao Wu

School of Resources and Environment, Henan University of Technology, Jiaozuo, Henan 454000, China

ABSTRACT

Impervious surface is an important indicator for analyzing urban expansion, measuring the degree of urbanization, and characterizing the urban ecological environment. Accurately extracting impervious surface data is of great significance to regional economic development, disaster prediction, ecological restoration, and environmental assessment. In this paper, using multi-spectral, synthetic aperture radar (SAR) and surface temperature retrieval (LST) data, from the four perspectives of spectral features, time series features, SAR texture features, and coherence features, an index feature that highlights impervious surface information is constructed. The model generates a 10m impervious surface product in the urban area of Shaoguan, and verifies the accuracy of the real sample based on the 0.8m GF-2 data in the same period. The results indicate that the overall accuracy of extracting impermeable surfaces in the study area is 94%, with a Kappa coefficient of 0.92. The multi feature fusion random forest model combining optical data and SAR data has high extraction accuracy and applicability in the mountainous areas of southwestern China, which improves the misclassification of bare land and other land types as impermeable surfaces.

KEYWORDS

Impervious surface; data fusion; SAR data; multi-feature; random forest.

1. INTRODUCTION

In the past three decades, the global urbanization process has rapidly developed, with over half of the global population now residing in urban areas. It is projected that by 2050, two-thirds of the global population will be living in cities [1]. Impervious Surface (IS) refers to natural and artificial surfaces that impede direct water infiltration into the soil, primarily composed of materials such as metal, glass, asphalt, and concrete, including building roofs, parking lots, and roads [2]. The rapid expansion of cities has led to a significant increase in impervious surfaces. In this scenario, a large amount of natural land surface is replaced by impervious surfaces, becoming a crucial surface cover type in urban land use. Impervious surfaces contribute to the urban heat island effect and are a critical indicator of urban ecological issues, directly affecting urban livability. Therefore, obtaining accurate, fast, and efficient information on the distribution of impervious surfaces in cities is of great significance in promoting the development of new urban areas, eco-cities, and sponge cities in China [3].

Currently, the extraction methods for impervious surfaces mainly include regression models[4], decision tree methods [5], deep learning methods [6], and index-based methods. The index-based method utilizes remote sensing indices to extract impervious surfaces. By identifying strong and weak reflectance bands of impervious surfaces within the multispectral range, new bands are constructed through combinations and operations, enhancing the information of impervious surfaces in the

generated index image. Various indices have been proposed in the literature for impervious surface extraction, such as the Normalized Difference Built-up Index (NDBI) [7], Enhancement Normalized Difference Impervious Surface Index (ENDISI) [8], and Improved Bareness Area Index (IBAI) [9].

In addition to the visible light bands utilized by the index-based method, the thermal infrared band can measure the surface's thermal radiation, allowing for the retrieval of Land Surface Temperature (LST). Impervious surfaces often exhibit different thermal characteristics from the surrounding environment due to their higher thermal capacity and conductivity. The extraction of low reflectance built-up areas using thermal infrared imagery is effective and can successfully eliminate the influence of water bodies and shadows. Azmi et al. demonstrated the impact of LST on impervious surfaces by considering local building types and climate conditions [10]. Yang et al. established a relationship model between LST and impervious surface area (ISA), analyzing the spatiotemporal changes and confirming the positive correlation between land surface temperature and impervious surfaces [11].

From a practical standpoint, optical remote sensing is a passive sensing technique that acquires information by receiving the reflected information or spectral energy radiated from objects. However, the reflected information of objects is inevitably influenced by lighting conditions and weather. On the other hand, Synthetic Aperture Radar (SAR) data has the advantages of all-day, all-weather capability, penetration through clouds, and vegetation coverage, making it uniquely advantageous for remote sensing monitoring in cloudy and rainy regions. SAR data provides rich texture information and is sensitive to surface moisture, which has a positive effect on the extraction of impervious surfaces. SAR remote sensing data can partially compensate for the limitations of optical and infrared remote sensing. By fusing SAR data with optical remote sensing data, the accuracy of impervious surface extraction can be improved. Zhu et al. combined Sentinel-1 SAR images with Sentinel-2 optical images to fully exploit the characteristic information of impervious surfaces, enhancing the ability to identify impervious surfaces in complex urban environments and successfully extracting impervious surfaces in Hainan Island [12]. Jiang et al. demonstrated the feasibility and potential of radar remote sensing in estimating impervious surface coverage in urban areas using the Classification and Regression Tree (CART) algorithm [13].

The extensive application of multi-source remote sensing data provides more options for research. Among them, the key to improving the classification accuracy of impervious surfaces lies in the use of image classification methods and multi-source data fusion methods. In this study, the research area is located in Shaoguan City, and Landsat 8/Sentinel-2 optical imagery data and Sentinel-1 SAR imagery data are used. The aim of the study is to explore the advantages and disadvantages of single data sources and multi-source remote sensing data fusion for extracting impervious surface information in the urban area of Shaoguan City.

2. RESEARCH AREA AND DATA SOURCES

2.1. Overview of Research Area Introduction

Shaoguan City is located in the northern part of Guangdong Province and serves as an important transportation hub in southern China. As of the end of 2022, the city had a total registered population of 2.86 million, with 1.66 million residing in urban areas, resulting in an urbanization rate of 58.13%. Shaoguan has a subtropical monsoon climate, with an average annual temperature of 21°C and an annual precipitation of around 1800mm. The average summer temperature ranges from 25-34°C. The unique climate of Shaoguan contributes to its cloudy and rainy conditions. For this study, we selected the three main urban areas of Zhenjiang District, Wujiang District, and Qujiang District in Shaoguan City (113°7′E-113°58′E and 24°27′N-25°5′N), with a total area of 2880km2. The study area exhibits diverse land cover types, including extensive vegetation (forests and farmland), bare land, water bodies, and residential areas.

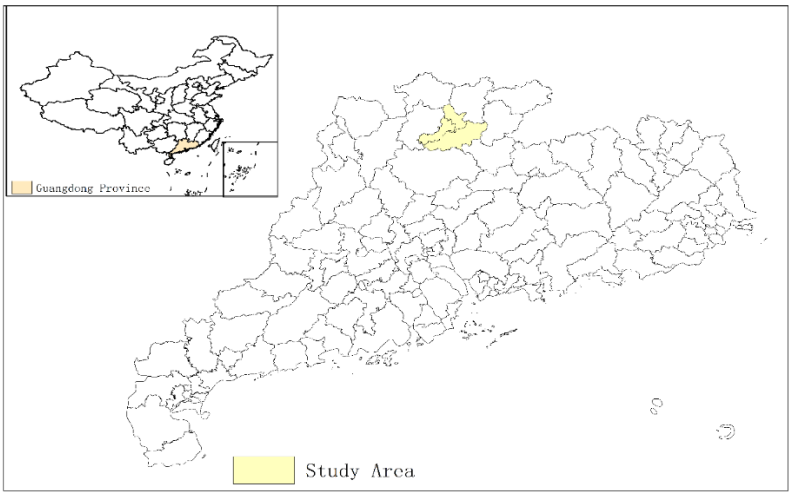

Figure 1. Location of the Study Area

2.2. Data source and preprocessing

(1) The Landsat 8-OLI/TIRS data is acquired from the United States Geological Survey (USGS) and was obtained on December 24, 2022, with low cloud cover and good atmospheric conditions. The data includes 30m multispectral data and a 15m resolution panchromatic band. The images have undergone pre-processing steps such as radiometric calibration, atmospheric correction, and mosaic cropping.

(2) Sentinel-2 MSI data. Sentinel-2 carries the Multi Spectral Instrument (MSI) and was successfully launched in 2015. It has a revisit period of 10 days and includes 13 spectral bands ranging from visible to near-infrared and shortwave infrared (SWIR). The highest resolution reaches up to 10m. The data used in this study was acquired on December 25, 2022, and is at level L2A, which has been radiometrically and atmospherically corrected to surface reflectance.

Table 1. Sentinel-2A MSI and Landsat8 OLI/TIRS data parameters

Landsat-8 (OLI/TRIS)			Sentinel-2A (MSI)		
Band	Center wavelength (μm)	Spatial resolution (m)	Band	Center wavelength (μm）	Spatial resolution (m)
Coastal	0.443	30	coastal	0.444	60
Blue	0.482	30	blue	0.497	10
Green	0.562	30	green	0.560	10
Red	0.655	30	red	0.665	10
near infrared (NIR)	0.865	30	vegetation red edge	0.704	20
shortwave infrared (SWIR 1)	1.609	30	vegetation red edge	0.740	20
shortwave infrared (SWIR 2)	2.201	30	vegetation red edge	0.783	20
Panchromatic	0.590	15	NIR	0.835	10
Cirrus	1.374	30	narrow NIR	0.865	20
thermal infrared (TIRS 1)	10.895	30	water-vapor	0.945	60
thermal infrared (TIRS 2)	12.005	30	SWIR cirrus	1.374	60
			SWIR	1.614	20
			SWIR	2.202	20

(3) Sentinel-1 SAR data. The Sentinel-1 satellite is part of the European Space Agency's Copernicus program and consists of two satellites carrying C-band Synthetic Aperture Radar (SAR). The revisit

period for the China region is 12 days. In this study, dual-polarization (VV+VH) and IW mode images from 2022 were used for the study area. The images have undergone thermal noise removal, radiometric calibration, and terrain correction. All the images were co-registered by mean compositing and cropped according to the study area extent.

The SAR and optical remote sensing data used in this study were acquired during the same period. The SAR data were geocoded and projected to the WGS 1984 coordinate system and UTM 49N projection, ensuring registration error control within 10m. The parameters of the Sentinel-2A MSI and Landsat 8 OLI/TIRS data used in this study are shown in Table 1.

3. RESEARCH METHOD

3.1. Technology Roadmap

The study aims to extract impervious surfaces in the main urban area of Shaoguan by integrating Landsat 8-OLI/TIRS, Sentinel-1, and Sentinel-2A data. The main extraction workflow is as follows:①Preprocessing: Preprocess the multi-source data.②Sample library construction: Build a sample library for Shaoguan through manual interpretation, including training and validation samples.③Multi-dimensional feature extraction: Extract multi-dimensional features of impervious surfaces from the perspectives of spectral, temporal, SAR texture, and coherence information using the multi-source data.④Model construction: Select model parameters and input features and establish a random forest model for impervious surface extraction.⑤Accuracy assessment: Evaluate the accuracy of the extraction results and compare them with existing datasets.

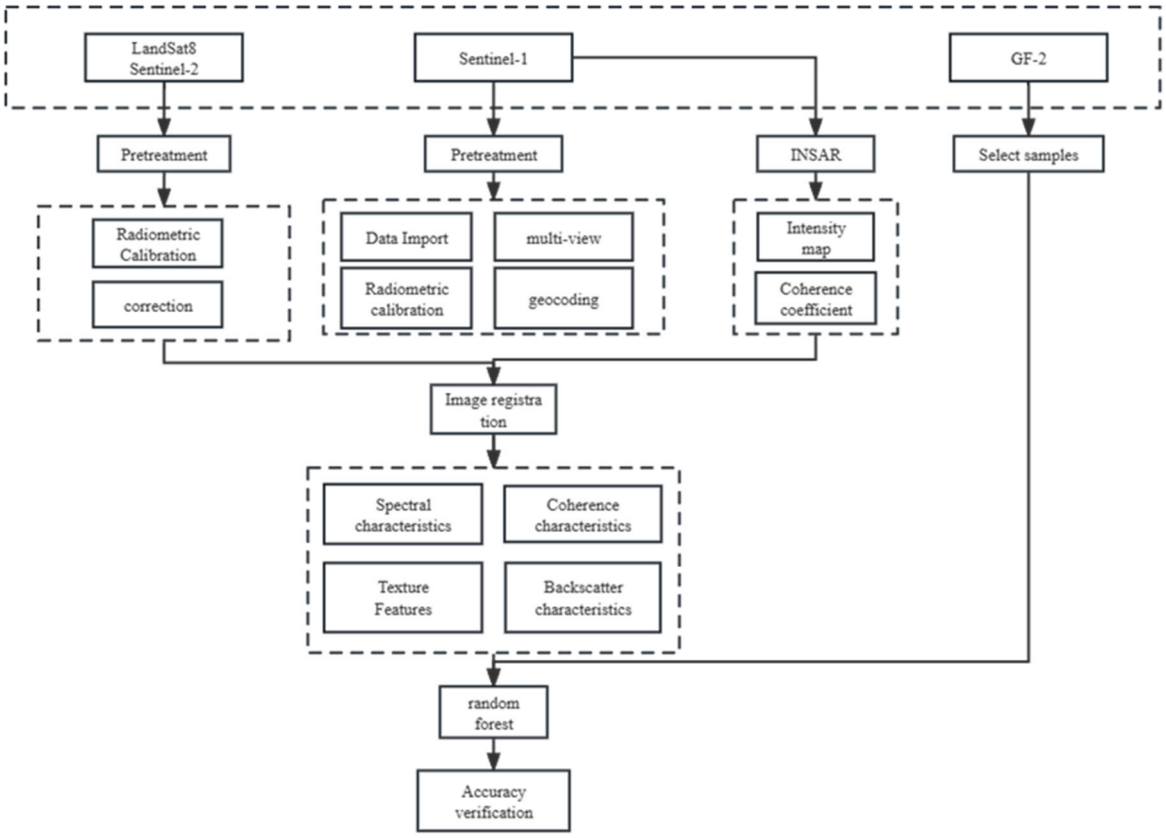

Figure 2. Flow chart of Random forest impervious surface extraction algorithm based on multisource data and multi features

3.2. Feature Extraction

Different land covers have varying absorption and reflection characteristics for different wavelengths of light. By utilizing algebraic operations between bands, the spectral information of target land covers can be enhanced, allowing for effective discrimination between target land covers and other land covers.

The spectral features extracted from Sentinel-2 imagery include the blue band (Blue), green band (Green), red band (Red), near-infrared band (NIR), shortwave infrared bands (SWIR1, SWIR2), as well as the Enhanced Normalized Difference Impervious Surface Index (ENDISI), Modified Normalized Difference Water Index (MNDWI), and Normalized Difference Vegetation Index (NDVI). These features provide valuable insights for analyzing land cover characteristics and distinguishing impervious surfaces, water bodies, and vegetation.

In the equation, "green" represents reflectance in the green band, "blue" represents reflectance in the blue band, "red" represents reflectance in the red band, "nir" represents reflectance in the near-infrared band, and "swir1" and "swir2" represent reflectance in the shortwave infrared bands.

$$MNDWI = \frac{(\text{green} - \text{swir1})}{(\text{green} + \text{swir1})} \tag{1}$$

$$ENDISI = \frac{\frac{2 * blue + swir2}{2} - \frac{red + nir + swir1}{3}}{\frac{2 * blue + swir2}{2} + \frac{red + nir + swir1}{3}} \tag{2}$$

$$NDVI = \frac{(\text{green} - \text{swir1})}{(\text{green} + \text{swir1})} \tag{3}$$

In the formula, green represents the green band reflectance; Blue is the reflectance of the blue band; Red is the red reflectance; NIR represents near-infrared reflection; Swir1 and Swir2 are the reflectivity in the shortwave infrared band.

Principal Component Analysis (PCA) is an effective method for feature extraction. It reduces the number of features while preserving the maximum amount of information from the original data, thus improving computational efficiency. Applying PCA to Sentinel-2 data can identify the optimal bands for image classification. After performing PCA, the first component (PCA1) contains the most significant amount of information, highest contrast, and variance. PCA1 can effectively differentiate impervious surfaces from other land cover classes.

3.2.1. Time Series Characteristics

NDVI is commonly used to reflect vegetation growth status and vegetation cover. The NDVI of impervious surfaces is generally not influenced by seasons, while croplands and other vegetation exhibit significant variations in NDVI across different seasons. Therefore, using NDVI time-series data can effectively distinguish impervious surfaces from croplands and vegetation.

In this study, data from the three months before and after the experimental period were selected. The NDVI index was calculated for each image. Then, all the NDVI values were sorted, and the sorted NDVI mean (NDVI_Mean) and standard deviation (NDVI_StdDev) were computed. These two statistical measures will serve as the temporal feature bands for the model.

3.2.2. Texture Features

Impervious surfaces and bare land share similar spectral characteristics, making it difficult to distinguish them using only the aforementioned features. Texture features, on the other hand, analyze

the distribution of grayscale levels, pixel differences, similarities, and roughness in an image, providing detailed and local information that may not be captured by spectral features alone [14] Research has found a correlation between SAR (Synthetic Aperture Radar) texture features and impervious surfaces. Based on the characteristics of HH (horizontal transmit and horizontal receive) and VV (vertical transmit and vertical receive) images, texture features based on VV images have been determined. SAR features reflect geometric and scattering characteristics of the terrain, which can amplify the differences between impervious surfaces and water bodies, vegetation, and other land features.

Studies have shown that SAR texture features provide more abundant information compared to multispectral imagery [15]. In this study, commonly used VV texture features, namely VV_Mean, VV_Contrast, and VV_Dissimilarity, were computed using the glcmTexture() function.

3.2.3. Coherence Characteristics

Based on the coherence coefficient, impervious surfaces primarily consist of infrastructure such as roads and buildings, which exhibit minimal changes over the time interval. The main and auxiliary images receive signals that are nearly identical, resulting in high coherence coefficient values. On the other hand, permeable surfaces are mainly composed of vegetation and water bodies, which experience significant variations due to factors like wind and seasons within the time interval. Consequently, permeable surfaces exhibit lower coherence coefficient values. Therefore, the differences in coherence coefficient between different land features in radar interferometry data can be utilized for impervious surface extraction.

Table 2. Impervious surface extraction feature set

Number	Feature Name	Meaning of features	Features and uses	category
1	NDVI	Normalized Difference Vegetation Index	Distinguishing between vegetation and non vegetation	Spectral characteristics
2	MSWI	Normalized Difference Water Index	Distinguishing between water and non water bodies	
3	ENDISI	Enhanced normalization with poor transparency Water surface index	Distinguishing between bare soil and impermeable surfaces	
4	PCA1	First principal component band	Enhanced extraction of impermeable surfaces	
5	LST	Surface temperature		
6	B8	8th band reflectance		
7	NDVI_Mean	Time series NDVI average value	Distinguish between cultivated land and wasteland with seasonal vegetation cover	timing characteristics
8	NDVI_StdDev	Time series NDVI standard deviation		
9	VV	极化波段		SAR
10	VV_Contrast	Contrast based on VV images	Enhanced extraction of impermeable surfaces	Texture Features
11	VV_Mean	Average based on VV images		
12	VV_Dissimilarity	Heterogeneity based on VV images		
13	VV_cc	Coherence based on VV images		Coherence characteristics

3.3. Random Forest Model

Random Forest (RF) algorithm is an ensemble algorithm based on decision trees, where each decision tree is independently distributed and the decisions made by each tree do not interfere with each other. When classifying samples using Random Forest, each decision tree makes a judgment on the input sample, and the final classification result is determined by the majority vote of multiple tree classifiers.

The experimental features of the Random Forest algorithm are selected from the total feature pool, preventing overfitting of the model. Random Forest has high accuracy for high-dimensional data and does not require feature selection, making it highly applicable for the multi-feature fusion in this study.

3.4. Feature Selection

In remote sensing image classification, feature selection and optimization play a crucial role. Including all features in the classification process can lead to information redundancy and even dimensionality catastrophe, which can adversely affect the improvement of classification accuracy. Therefore, feature selection can be used to reduce data dimensionality and improve the model's generalizability. Random Forest algorithm is an effective method in machine learning for handling high-dimensional data. It can not only classify image pixels but also evaluate the contribution of feature variables in predicting the target variable through feature importance.

In this study, feature importance scoring is achieved using the Random Forest algorithm. The specific process involves calculating the error of each decision tree in the Random Forest using the corresponding out-of-bag (OOB) samples. Then, noise is added to the features of all OOB samples randomly, and the OOB error is recalculated. Assuming the Random Forest has N trees, the feature importance score for a particular feature is determined by observing a significant decrease in the accuracy of the OOB after adding noise, indicating a strong influence of that feature on the classification results and a high importance score. Feature selection is performed by cumulatively adding features in descending order of their importance scores,

3.5. Extraction accuracy evaluation

The study evaluates the accuracy of different feature combination methods by constructing a confusion matrix. The test sample set and validation sample set are obtained through visual interpretation of GF-2 images from the same period. The confusion matrix is calculated based on the sample point data. The specific accuracy evaluation metrics include Producer's Accuracy, User's Accuracy, Overall Accuracy, and Kappa coefficient[16].

4. RESULTS AND ANALYSIS

4.1. Spectral analysis of different land features

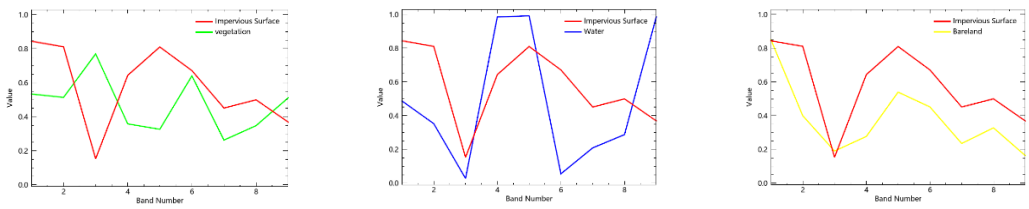

Figure 3. Normalized Spectral Curves of Impervious Surface, Water Body, Vegetation, and Naked Land under Extracting Feature Set

According to the feature set extracted from multisource remote sensing data in the study area (Figure 3), impervious surfaces, water bodies, vegetation, and bare land show significant differentiation in different features. Under Band 1 (LST), impervious surfaces and bare land exhibit higher temperatures and can be well distinguished from water bodies and vegetation within the rule set. In Band 2 (coherence coefficient band), there is distinct differentiation between impervious surfaces and other land cover types. Under the Band 3 (NDVI) feature, there is significant differentiation between vegetation and impervious surfaces. In Band 4 (MNDWI band), water bodies exhibit significant differences from other land cover types. Under Band 5 (ENDISI), there is notable differentiation in the curves between impervious surfaces and other land cover types. Through the reflection of different land cover types under the texture features of Bands 6, 7, and 8, the differences between impervious surfaces and other land cover types can be clearly observed. In Band 9 (PCA1), the differentiation of information among different land cover types can be reflected through the first component of the principal component analysis. Figure 3 analysis demonstrates the feasibility of extracting impervious surface datasets.

4.2. Feature Selection Analysis

We'll use random forest to calculate importance scores for different variables in the feature combination. Then, in the classification process, we'll incrementally add variables with high importance scores, starting from the highest, to achieve the highest classification accuracy. Using Scheme 6 as an example, we'll analyze the relationship between the number of selected feature variables and the overall classification accuracy and Kappa coefficient. This helps identify the optimal number of features and the best feature set for classification.

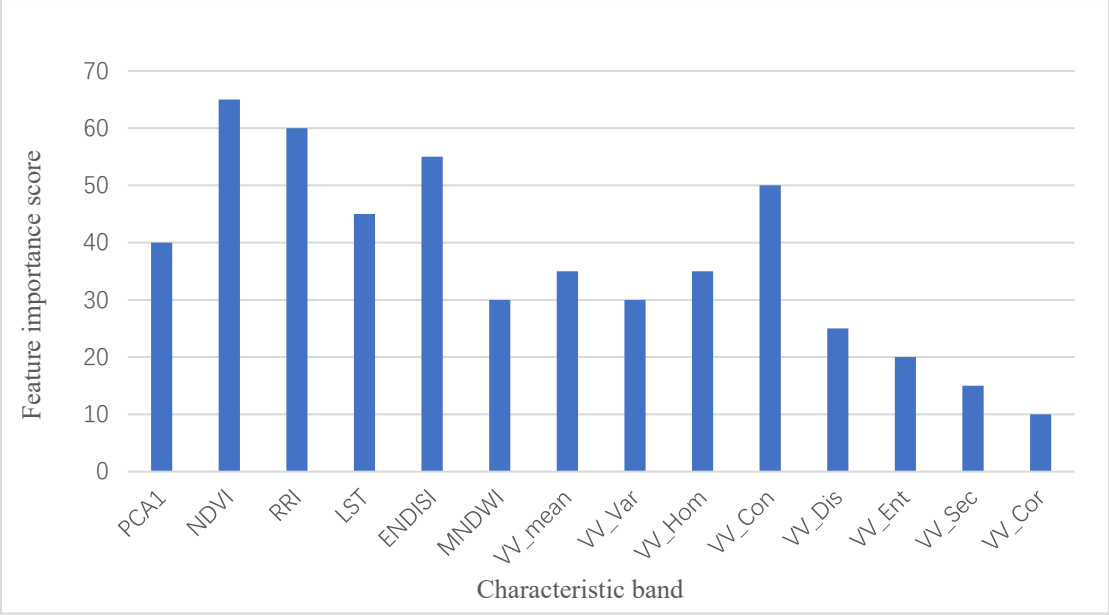

Figure 4. Ranking of Importance of Random Forest Features

4.3. Comparison of Different Feature Fusion Extraction Results

Based on the actual conditions of the study area and a review of the literature, the cover types of the study area are divided into four types: impervious surfaces, water bodies, vegetation, and bare land. By extracting 70% as training samples and 30% as validation samples.

Table 3. Classification of Object Names, Training Samples, and Accuracy Verification Samples

Land objects	Training sample pixels	Verify sample pixels
Impervious Surface	350	150
Bare Land	350	150
Vegetation	350	150
Water	350	150

To verify the extraction effect of impervious surfaces under the condition of inputting different features, this study designed an impervious surface extraction experiment based on a Random Forest model with multiple feature combinations. Experiment one is based on spectral features; experiment two is based on spectral features and temporal NDVI features; experiment three is based on spectral features, temporal NDVI features, coherence features, and SAR texture features. Through the experiments, the extraction accuracies under different feature conditions were obtained (Table 4). The experiments show that with the addition of different features into the Random Forest model, the extraction accuracy of impervious surfaces continuously improves. Compared to experiments one and two, the overall accuracy of impervious surface extraction in experiment three increased by 6%, yielding the best extraction effect.

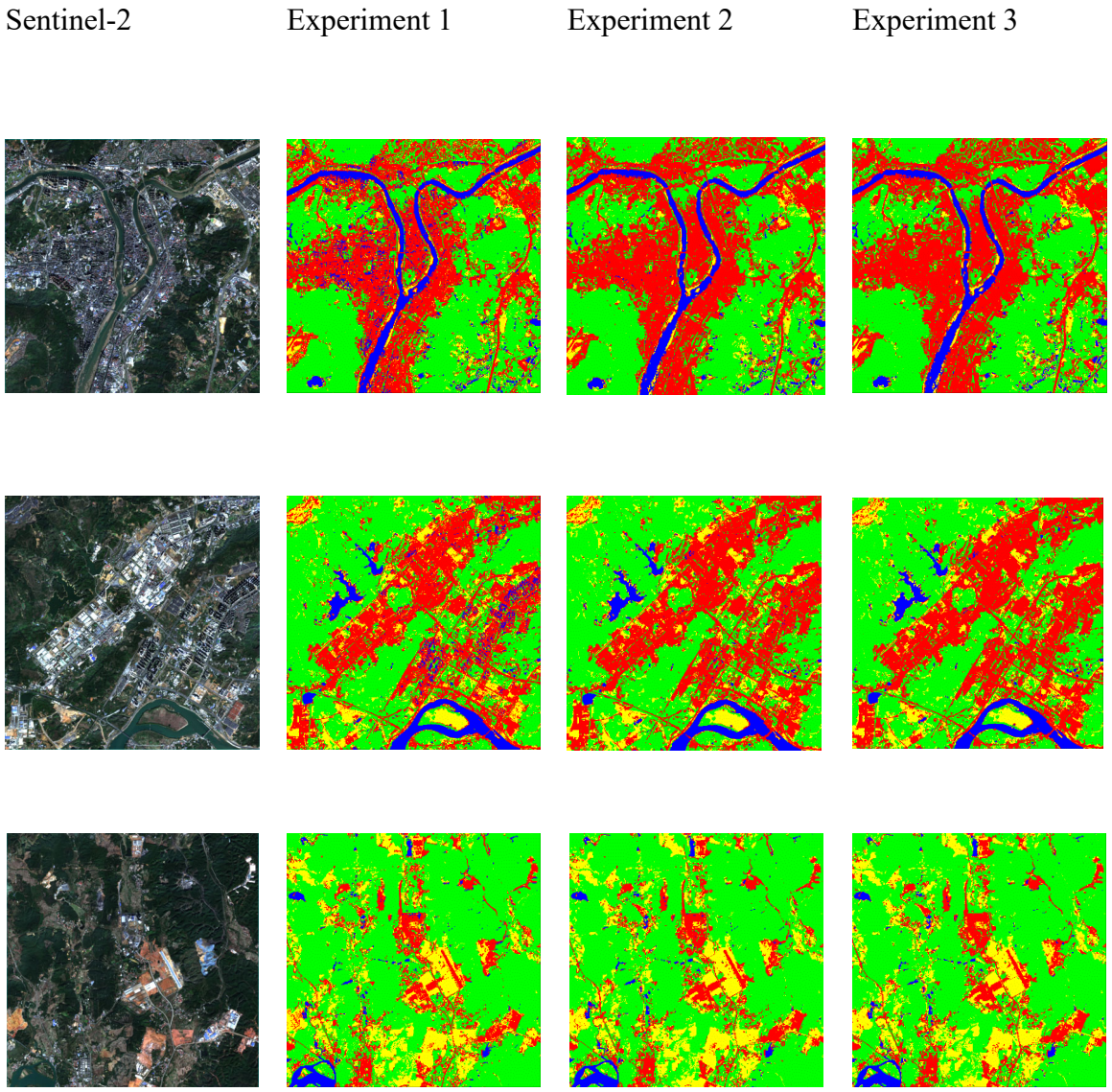

Figure 5. Impervious surface extraction results under different input characteristics

Table 4. Experimental Extraction Accuracy

	overall accuracy %	Kappa coefficient%	Producer's accuracy %	User Accuracy %
Experiment 1	88.75	0.85	83	79.81
Experiment 2	92.75	0.90	93	86.11
Experiment 3	94	0.92	94.67	91.88

Combining the analysis of Figure 5 and Table 4, it can be concluded that: 1) Spectral features are quite prominent for the extraction of large-scale impervious surfaces, allowing for relatively accurate distinction between impervious surfaces, water bodies, vegetation, and other features. However, due to the obstruction of buildings and the spectral similarity among impervious surfaces, bare land, and sandy soil, there are poor extraction effects in areas with building shadows and complex types of land cover. 2) Temporal NDVI can reflect the change in vegetation over time, with significant NDVI variations from bare land to cultivated land, thus incorporating temporal NDVI features can reduce the difficulty of identifying uncultivated land. 3) The change in urban impervious surfaces over a certain period is minimal, with high coherence; whereas vegetation, water bodies, and other features show greater changes in coherence over time. The scattering wave characteristics and dielectric properties of impervious surfaces result in significantly different backscattering signals from impervious surfaces compared to other land covers. In the experiments, SAR texture features were utilized to distinguish impervious surfaces from bare land effectively. Overall, compared to original bands, an extraction method that integrates multiple features from multispectral and SAR images can enhance the differentiation between impervious surfaces and bare soil, effectively improving the accuracy of impervious surface extraction.

For this study, GF-2 image data from the same period were chosen as the real images, and a confusion matrix analysis was performed using 400 randomly selected land cover sample points as the real images to obtain accuracy verification data. The overall extraction accuracy of impervious surfaces in the main urban area of Shaoguan City was 94%, with a Kappa coefficient of 0.92, indicating good differentiation and high extraction accuracy.

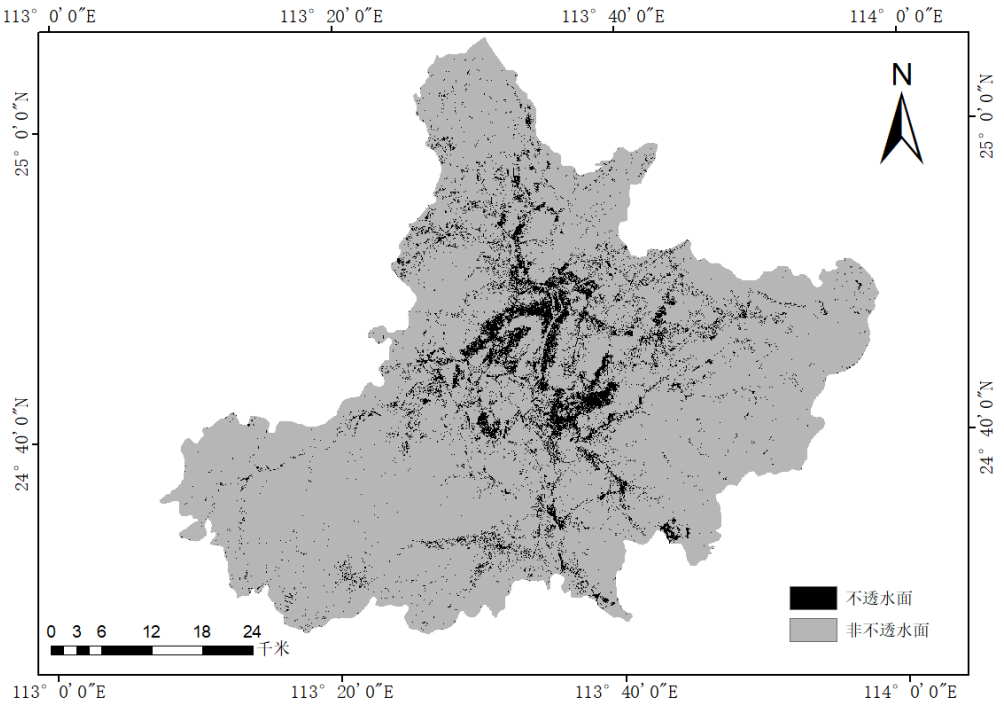

Figure 5. Distribution of impervious surface in main urban area of Shaoguan City

By merging vegetation, bare soil, and water bodies into non-impervious surfaces, the distribution of impervious surfaces in the main urban area of Shaoguan City is obtained (Figure 5). The impervious surfaces in Shaoguan City are mainly distributed along the banks of the Qujiang, Beijiang, and Nan Shui rivers, as well as the Maba Shui and Zhangshi Shui, which are tributaries of the Beijiang River. The total area of impervious surfaces accounts for approximately 8.6% of the main urban area of Shaoguan City. Within the non-impervious surfaces, vegetation accounts for about 81.2%, indicating that Shaoguan City has a relatively low urbanization rate and a high vegetation coverage rate.

4.4. Comparison with impermeable surface data products

To verify the accuracy of the extraction results in the study area, the most recent impervious surface data product, GIAI 1985-2022[17], updated to coincide with the study period of this paper in 2022, was selected for accuracy comparison.

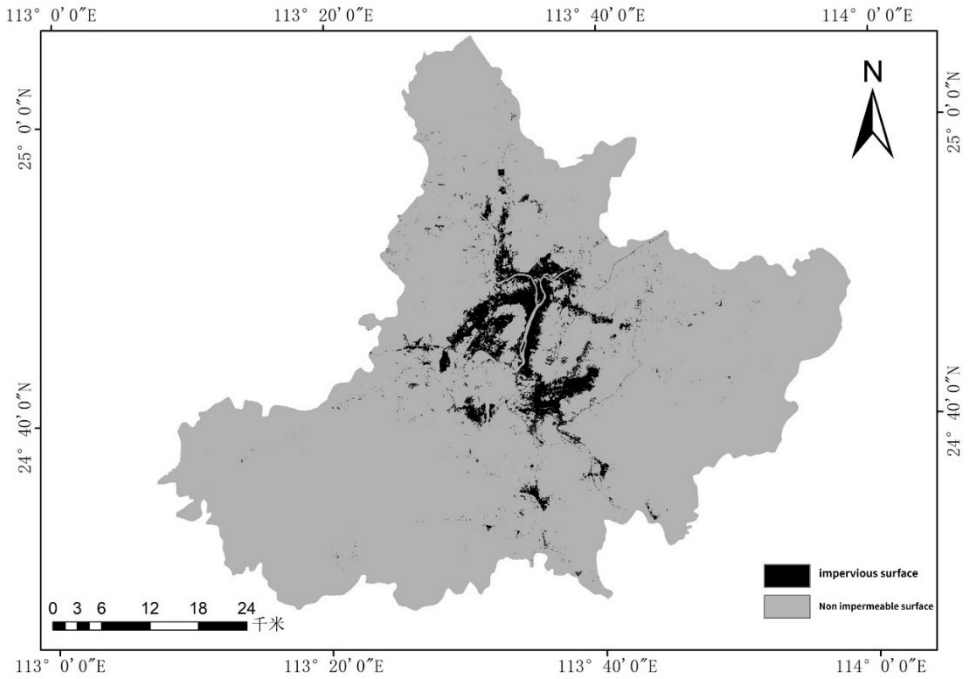

Figure 6. GIAI dataset: impervious surface distribution in the main urban area of Shaoguan City

Upon verification, the overall accuracy of the GIAI data product for impervious surface extraction within the study area was 90.75%, with a Kappa coefficient of 0.9. The comparison reveals that the extraction accuracy of the method proposed in this paper significantly improves over existing impervious surface datasets. The GIAI product performs poorly in extracting small patches of impervious surfaces within urban and mountainous areas.

5. CONCLUSION

This study, based on Landsat 8, Sentinel-2 multispectral, and Sentinel-1 SAR data, proposes an extraction method using a Random Forest model that integrates spectral, temporal, SAR texture features, and coherence features for extracting impervious surface information in the main urban area of Shaoguan. The results are as follows:

(1) Compared to the extraction of impervious surfaces using only spectral features, which can lead to over-extraction and under-extraction, the Random Forest model integrating spectral features,

temporal features, SAR texture features, and coherence features demonstrates better extraction performance. The fusion of multi-source data provides various types of information that effectively improve classification accuracy.

(2) Compared with the existing contemporaneous impervious surface product dataset (GIAI 1985-2022), the overall accuracy has improved by 4%, showing better extraction performance in urban areas, mountainous areas, and regions with small patches of impervious surfaces.

(3) The total area of impervious surfaces in the main urban area of Shaoguan City is 247.7 km², accounting for 8.6% of the main urban area, with an overall extraction accuracy of 94% and a Kappa coefficient of 0.92. Impervious surfaces are mainly distributed in low-elevation areas around the main streams of Qujiang, Beijiang, and tributaries of Beijiang in Shaoguan City. Areas far from rivers have less impervious surface distribution due to topographical reasons.

REFERENCES

[1] Cohen B .Urbanization in developing countries: Current trends, future projections, and key challenges for sustainability[J].Operations Research, 2006.

[2] Arnold Jr C L, Gibbons C J. Impervious surface coverage: The emergence of a key environmental indicator[J]. Journal of the American Planning Association, 1996,62(2): 243-258.

[3] He Yunhai, Guo Qiaozhen, Qiao Yue, Wu Huanhuan, Zhu Li. Research on Extracting Impervious Surface from High Resolution VI Images [J]. Surveying and Mapping Science,2022,47(09):138-145.

[4] XIANG Chao, ZHU Xiang, HU Deyong, et al. Monitoring the Impervious Surface with Multi-resource Remote Sensing Images in Beijing-Tianjin-Tangshan Urban Agglomeration in the Past Two Decades[J]. Journal of Geo-information Science, 2018, 20(5): 684-693.

[5] Xian G, Crane M. Assessments of urban growth in The Tam - pa Bay Watershed using remote sensing data［J］. Remote Sensing of Environment, 2005, 97 (2): 203-215.

[6] PATEL N, MUKHERJEE R. Extraction of Impervious Features from Spectral Indices using Artificial Neural Network[J]. Arabian Journal of Geosciences, 2015, 8(6): 3729-3741.

[7] Zha Y, Ni S X, Yang S. An effective method for automatically extracting urban land use Infor-mation using TM images[J]. Journal of Remote Sensing, 2003,7(1):37-40.

[8] Mu Yachao, Jie Yaowen, Zhang Lingling, Chen Yunhai. A new enhanced impermeability index [J]. Surveying and Mapping Science,2018,43(02):83-87.

[9] Zhang Kaixuan, Xu Na, Li Xiuhui, Yin Zhuo, Tu Liying. A comprehensive index for extracting impermeable water surfaces [J]. Surveying and Mapping Science,2022,47(10):153-160.

[10] Azmi, Rida, Abderrahim Saadane, and Ilias Kacimi. "Estimation of spatial distribution and temporal variability of land surface temperature over Casablanca and the surroundings of the city." International Journal of Innovation and Applied Studies 11.1 (2015): 49-57.

[11] Yang, Qiquan, et al. "The relationship between land surface temperature and artificial impervious surface fraction in 682 global cities: spatiotemporal variations and drivers." Environmental Research Letters 16.2 (2021): 024032

[12] Zhu Xiulin, Zhao Xiangwei, Du Wenjie, Sun Zhongchang. Urban Impervious Surface Dataset of Hainan Island Based on Sentinel-1 SAR and Sentinel-2A Optical Images [J]. Chinese Science Data (Chinese English online version) ,2019,4(02):69-80.

[13] Jiang Liming, Liao Mingsheng, Lin Hui, Yang Limin, Wang Changcheng. Estimation of the percentage of urban impermeable layers using radar interference data [J]. Journal of Remote Sensing,2008(01):176-185.

[14] Haralick R M .Textural features for image classification. IEEE Transaction on Systems, Man, and Cybernetics [J]. SMC, 1973, 3.

[15] Zhang Y , Zhang H, Lin H. Improving the impervious surface estimation with combined use of optical and SAR remote sens- ing images [J]. Remote Sensing of Environment. 2014, 141: 155-167.

[16] Liaw A, Wiener M. Classification and regression by random - forest [J]. R news, 2002, 2 (3): 18-22.

[17] Gong P , Li X , Wang J ,et al.Annual maps of global artificial impervious area (GAIA) between 1985 and 2018[J].Remote Sensing of Environment, 2020.